Micromachined Accelerometer Design, Modeling and Validation

*Brady R. Davies, Vesta I. Bateman, Frederick A. Brown, Stephen Montague, James R. Murray, Danny Rey, James H. Smith
Sandia National Laboratories
http://www.mdl.sandia.gov/Micromachine

Abstract

Micromachining technologies enable the development of low-cost devices capable of sensing motion in a reliable and accurate manner. The development of various surface micromachined accelerometers and gyroscopes to sense motion is an ongoing activity at Sandia National Laboratories. In addition, Sandia has developed a fabrication process for integrating both the micromechanical structures and microelectronics circuitry of Micro-Electro-Mechanical Systems (MEMS) on the same chip. This integrated surface micromachining process provides substantial performance and reliability advantages in the development of MEMS accelerometers and gyros.

A Sandia MEMS team developed a single-axis, micromachined silicon accelerometer capable of surviving and measuring very high accelerations, up to 50,000 times the acceleration due to gravity or 50 k-G (actually measured to 46,000 G). The Sandia integrated surface micromachining process was selected for fabrication of the sensor due to the extreme measurement sensitivity potential associated with integrated microelectronics. Measurement electronics capable of measuring attoFarad (10^{-18} Farad) changes in capacitance were required due to the very small accelerometer proof mass ($<200 \times 10^{-9}$ gram) used in this surface micromachining process. The small proof mass corresponded to small sensor deflections which in turn required very sensitive electronics to enable accurate acceleration measurement over a range of 1 to 50 k-G. A prototype sensor, based on a suspended plate mass configuration, was developed and the details of the design, modeling, and validation of the device will be presented in this paper. The device was analyzed using both conventional lumped parameter modeling techniques and finite element analysis tools. The device was tested and performed well over its design range.

I. Introduction

The acceleration environment experienced by the sensors and electronics in some high shock environments is extreme, with average accelerations in the 20,000-G range and peak transient accelerations up to several hundred thousand G[1]. Commercially available accelerometers used in shock testing of earth-penetrator weapons components are both expensive ($1800 each) and prone to failure.

The only reported silicon-based high-G accelerometers are bulk-micromachined. Preliminary failure analysis of these commercial sensors indicated that failure modes included both undamped high-frequency resonances of the sensor itself and catastrophic failure of the packaging[2].

Specification for the nominal parallel-plate capacitance of the 50 kG sensor was 100 fF at a 2 μm gap. This capacitance level was constrained by the necessity to interface with an existing CMOS microelectronics design. When no acceleration was applied to the sensor, its nominal capacitance requirement constrained both the gap spacing and plate overlap area. This translated into a plate overlap area of ≅ 22, 500 μm^2 (≅ 150 μm x 150 μm square area), where the no-acceleration state gap spacing was constrained by the 2 μm thick sacrificial oxide layer used in the fabrication process. The desired gap spacing during acceleration of 50 kG was 1 μm. The resonant frequency of the sensor suspension was constrained to be greater than 100 kHz to accommodate sampling frequencies and the induced vibration caused by the sampling voltage electrostatic attractive force. To obtain adequate response, a target range of 0.7 for the damping ratio was desired. Damping was significantly constrained by fabrication considerations, specifically the requirement for sufficient spacing of etch- release holes. In this case,

* Sandia is a multiprogram laboratory operated by Sandia Corporation, a Lockheed Martin Company, for the United States Department of Energy under Contract DE-AC04-94AL85000.

there was very little design flexibility to control damping using the mechanism of squeeze-film damping of the air surrounding the sensor and a much lower damping ratio was realized.

II. High-G Accelerometer Modeling

A suspended mass, high-G accelerometer was designed and fabricated in a variation of Sandia's integrated surface-micromachined polysilicon with electronics manufacturing process[3]. This sensor consists of a parallel-plate capacitor, with one plate stationary with respect to the sensor housing and the second plate suspended by flexible beams that deflect in proportion to the magnitude of the acceleration imposed upon the sensor housing. The sensor was designed to measure accelerations up to 50 k-G. Dominant design tradeoffs include balancing acceptable signal-to-noise ratios with stiff mass suspension elements. Another design challenge was to optimize damped response subject to processing constraints.

The mechanical elements of the high-G accelerometer were fabricated using two layers of polycrystalline silicon separated by 2 μm. The upper layer contained the moving mechanical element of the sensor, and the bottom layer acted as both a structural and electrical ground. The sensor principle of operation was to measure capacitance changes between the two plates with CMOS electronics located adjacent to the mechanical elements (same substrate).

Sensor deflection was modeled using lumped parameter approximations and conventional beam deflection theory. This type of analysis resulted in predicted maximum proof mass deflection at 50 k-G of 0.97 μm, damping ratio equivalent to approximately 0.45, and a natural frequency of 101 kHz. During design of the structure, it became apparent that the damping ratio was constrained by fabrication considerations, specifically the requirement for sufficient spacing of etch-release holes.

Damping was modeled by simultaneously applying three different models of squeeze film damping, each of which models some but not all of the applicable characteristics of the suspended mass prototype. Squeeze-film damping can be defined as the viscous loss of energy due to pumping a viscous fluid out from or into the volume between two moving surfaces.

The first model[4] is applicable to squeeze-film damping between two parallel disks without perforations, and the damping resistance, R_{film}, is characterized by the following equation:

$$R_{film} = 3\mu S^2/2\pi\delta^3 \text{ (N-s/m)} \quad (1)$$

where μ is the fluid viscosity (18×10^{-6} kg/m-s for air at 20 °C), S the plate area overlap, and δ the average plate spacing.

The second model[4] is applicable to squeeze-film damping when one plate is perforated, and the damping resistance, R_{perf}, is characterized by the following equation:

$$R_{perf} = 12\mu S^2/N\pi\delta^3 G(A) \text{ (N-s/m)} \quad (2)$$

where A is the fraction of open area in the plate, and N is the total number of holes in the perforated plate. The function G(A) is described in equation (3).

$$G(A) = [A/2 - A^2/8 - (\ln A)/4 - 3/8] \quad (3)$$

The third model[4] is applicable to squeeze-film damping at high frequencies (> 10 kHz). This viscous resistance is called radiation resistance and is characterized by the following equation:

$$R_{rad} = \rho c(A\omega/c)^2 \text{ (N-s/m)} \quad (4)$$

where ρ and c are the density and speed of sound of the viscous fluid, and ω is the frequency of motion. For the purposes of this research, each of the three models was applied to the design of the suspended mass accelerometer by modeling their respective damping contributions and combining them as parallel resistances. Thus, over the expected operating conditions of the accelerometer, different modeling parameters would result in different models dominating predicted damping resistance.

III. High-G Accelerometer Design

Designs for both the mechanical and electrical portions of the accelerometer were developed and fabricated using the Sandia integrated process. A layout (using the AutoCAD® CAD tool) for the mechanical design is shown in Figure 1. Compliance in both the vertical and horizontal directions was necessary in order for the sensor to perform properly. Horizontal compliance provided by the bent beams relieved residual stress that remains in structural polycrystalline silicon after processing. Vertical compliance was necessary so that sensor capacitance would change proportionally with acceleration.

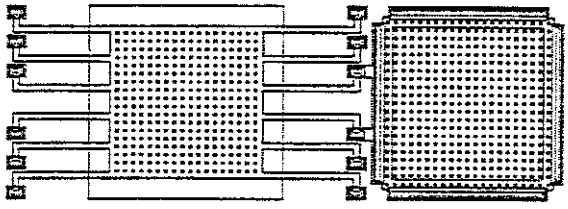

Figure 1: Bent Beam Design for High-G Accelerometer

The CMOS circuitry for the accelerometer consists of a unity gain buffer followed by a multiplier and low-pass filter. The purpose of the circuit is to measure the change in capacitance of the sensor capacitor relative to the fixed reference capacitor (Figure 1). The sensor capacitor and the reference capacitor are connected in series and an AC signal is applied across the pair. If the two capacitors are not equal, an output signal appears at the common node of the pair. This signal is proportional to the acceleration and is sensed by the CMOS circuit.

The multiplier stage is used to demodulate the signal from the buffer. The buffer output is multiplied by the AC signal that was applied to the sensor. In effect the output of the buffer is an AM signal. The AC input signal applied to the sensor is the carrier and the acceleration is the data. The input differential amplifiers use source followers as loads to predistort the data to maximize the linearity of the multiplier.

The low-pass filter is a second order active filter. The cutoff frequency of the filter is 50 kHz. This Butterworth filter is designed to eliminate any switching noise from the multiplier. The output stage of the op amp is designed to drive loads down to 1 kΩ. When a 100 kG acceleration is applied to the device the sensor capacitor should increase from 100 fF to 200 fF. For this acceleration, the amplitude of the waveform at the output of the filter will be 2 V. The gain of the CMOS circuit can be varied by changing the amplitude of the AC signal applied to the sensor.

IV. Finite Element Analysis of High-G Accelerometer

Finite element analysis software was used to verify the accelerometer mechanical design. The finite element software that was used is called ANSYS/AutoFEA® 3D, and is compatible with AutoCAD® generated geometry. Results of this analysis software predicted somewhat different deflection and resonant frequency values than those obtained through analytical analysis (the analytical analysis was based on clamped beam theory). The software predicted that the structure would resonate at 151 kHz (Table 1) as compared to the manual analysis prediction of 101 kHz. The finite element software predicted maximum deflection at 50 k-G of 0.64 microns (Figure 2) compared to 0.95 microns using analytical analysis techniques. Additionally, finite element software predicted a maximum principal stress level of 93.2 MPa (Table 1) at 50 k-G compared to 74 MPa using manual analysis techniques.

• Vibration Frequencies:	• Maximum Deflection
– Mode 1: 151 kHz	(@ 50 k-g's):
– Mode 2: 240 kHz	– 0.64 microns
– Mode 3: 470 kHz	• Maximum Stress
– Mode 4: 498 kHz	(@ 50 k-g's):
– Mode 5: 747 kHz	– 93.2 MPa
– Mode 6: 876 kHz	

Table 1: Finite Element Analysis Results (at 50 k-G)

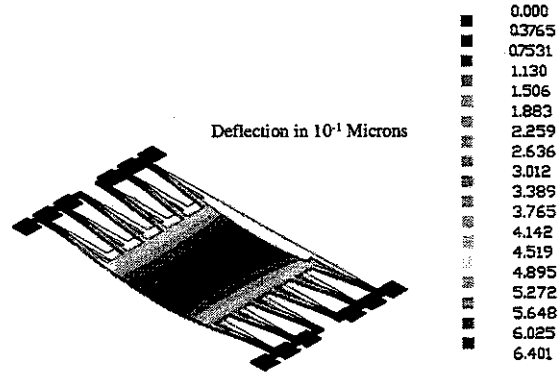

Figure 2: FEA of Sensor at 50 k-G

V. High-G Accelerometer Verification

The accelerometer was fabricated using the Sandia integrated micromachining and microelectronics process. Figure 3 below shows a Scanning Electron Microscope (SEM) photograph of the fabricated suspended plate mass accelerometer (inside square trench) with associated microelectronics (around the periphery) and reference capacitor (mechanically attached to the accelerometer).

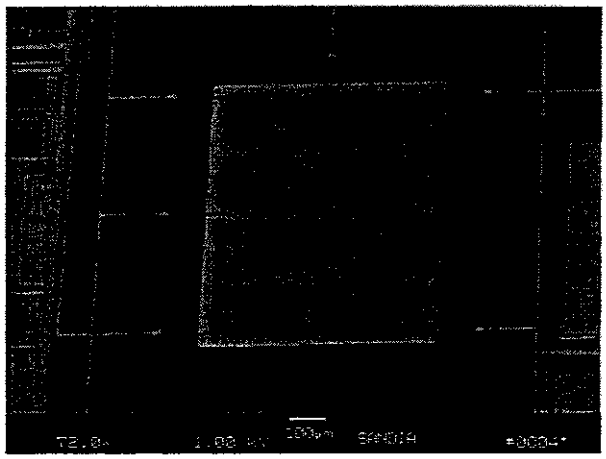

Figure 3: Scanning Electron Microscope Photograph of Fabricated Sensor

The high-G accelerometers were tested at a Hopkinson bar[5] shock facility, operated by Sandia's Manufacturing and Rapid Prototyping (Shock Testing) Department, which could provide shock inputs to the device as well as data acquisition and signal processing support for measurement data. A schematic diagram of the test circuitry is provided in Figure 4 below.

A test fixture was fabricated to mount the accelerometer IC to the Hopkinson bar test stand. Since wiring directly to the IC pins was necessary each time a new device was shock tested, a PC board was fabricated which facilitated direct mounting of the packaged sensor chip to the test fixture. Additionally, this allowed direct IC output monitoring which significantly improved reliability of the test setup.

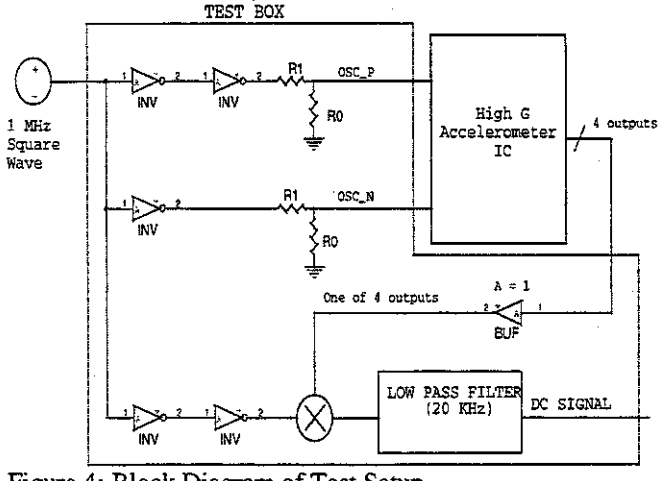

Figure 4: Block Diagram of Test Setup

A number of new failure modes were discovered once shock testing reached levels of 25,000 G and above. For instance, at 25,000 G, die adhesive failure was experienced that caused the chip to separate from the package during shock testing. This was traced to a chemical incompatibility introduced during the final etch release process. At approximately 40,000 G, the packages began to crack. This was corrected by modifying the lid seam sealing operation to reduce the mechanical stress concentrations coincident with the lid edges and modifying the mounting bracket to better distribute the mechanical stresses imposed by the bracket against the package during shock testing. These modifications corrected both the die adhesion and package cracking failures previously experienced.

Test results for the Sandia designed accelerometer were very positive, with the response of the sensor showing excellent correlation between the shock pulse and sensor output at accelerations up to 50,000 G (actually tested at 46,000 G). Filtered accelerometer response data is shown for a shock pulse of approximately 27 k-G in Figure 5.

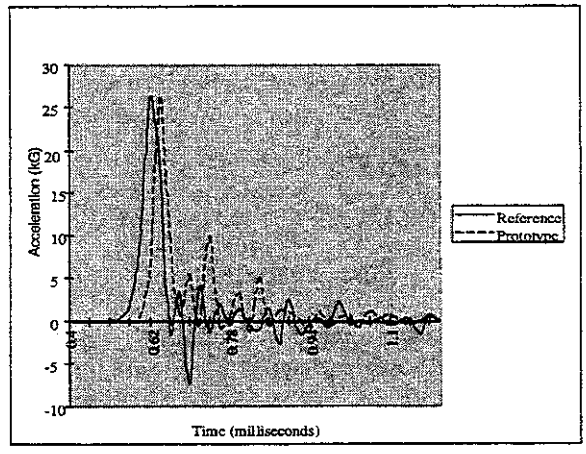

Figure 5: Filtered Acceleration vs. Time plot at 27 k-G

Figure 6 shows the filtered accelerometer response data for a shock pulse of approximately 46 k-G.

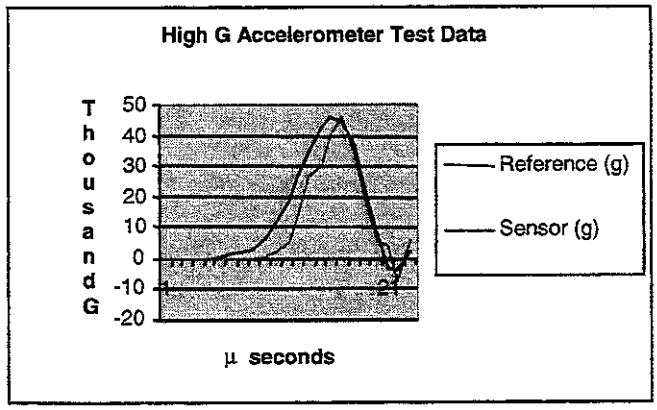

Figure 6: Filtered Acceleration vs. Time plot at 46 k-G

As seen in Figures 5 and 6, the initial shock pulse showed excellent correlation with the reference accelerometer in both magnitude and phase. After the initial pulse, further ringing of the structure resulted in diverging signals between the prototype accelerometer and reference accelerometer. The various vibrations and reflected pulses arrive at the respective accelerometers at different times and at different energies. This is due to the differences in location between the reference accelerometer and prototype accelerometer.

Table 2 below shows the shock pulse magnitudes and corresponding pulse durations for each shock test applied to the accelerometer. The device output correlated well with the acceleration input over the full range of pulse magnitude and duration test points.

Pulse Magnitude(G)	Pulse Duration (μseconds)
12,000	63
20,000	57
27,000	55
33,000	55
37,800	53
46,300	54

Table 2: Shock Magnitude vs. Pulse Duration

VI. Summary

The mechanical sensor element, supporting microelectronics, and packaging have been proven to operate properly at acceleration levels up to 46,000 G, with various modifications in the testing and packaging processes necessary to eliminate failures due to die adhesion and package cracking.

Ceramic packages proved to be a significant limitation at high shock levels. Plastic or stainless steel packaging might need to be substituted for ceramic packages, especially for future sensors that might be designed for accelerations exceeding 100 k-G.

Acknowlegements

The authors wish to thank the outstanding fabrication and engineering analysis contributions by the entire Microelectronics Development Laboratory (MDL) staff.

References

1. B. R. Davies, S. Montague, J. H.. Smith, M. Lemkin, "Micromechanical Structures and Microelectronics for Acceleration Sensing", Proceedings of SPIE Micromachining and Microfabrication Conference, *Micromachining and Microfabrication Process Technology III*, Volume 3223, pp 237-244, Sept., 1997.
2. T. Christenson, "Failure Analysis of Endevco 7270A High G Accelerometer", Sandia Internal Report, 1997.
3. J. Smith, S. Montague, J. J. Sniegowski, J. R. Murray, and P. J. McWhorter, "Embedded Micromechanical Devices for the Monolithic Integration of MEMS with CMOS," *IEDM Tech. Digest*, pp. 609-612, Dec. 1995.
4. T. B. Gabrielson, "Mechanical-Thermal Noise in Micromachined Acoustic and Vibration Sensors", *IEEE Transactions on Electron Devices*, Vol. 40, No. 5, May, 1993.
5. V. I. Bateman, R. G. Bell, and N. T. Davie, "Evaluation of Shock Isolation Techniques for a Piezoresisitive Accelerometer", *Proceedings of the 60th Shock and Vibration Symposium*, Volume I, November 14-16, 1989.